



The Arctic Ocean Manganese Cycle, an Overlooked Mechanism in the Anomalous Palaeomagnetic Sedimentary Record

Steffen Wiers^{1*}, Ian Snowball¹, Matt O'Regan², Christof Pearce³ and Bjarne Almqvist¹

¹ Department of Earth Sciences, Uppsala University, Uppsala, Sweden, ² Department of Geological Sciences, Stockholm University, Stockholm, Sweden, ³ Department of Geoscience and Arctic Research Centre, Aarhus University, Aarhus, Denmark

OPEN ACCESS

Edited by:

Juan Cruz Larrasoaña,
Geological and Mining Institute
of Spain, Spain

Reviewed by:

Luigi Jovane,
University of São Paulo, Brazil
Christian Ohnaiser,
University of Otago, New Zealand

*Correspondence:

Steffen Wiers
steffen.wiers@geo.uu.se

Specialty section:

This article was submitted to
Geomagnetism and Paleomagnetism,
a section of the journal
Frontiers in Earth Science

Received: 03 December 2019

Accepted: 28 February 2020

Published: 20 March 2020

Citation:

Wiers S, Snowball I, O'Regan M,
Pearce C and Almqvist B (2020) The
Arctic Ocean Manganese Cycle, an
Overlooked Mechanism
in the Anomalous Palaeomagnetic
Sedimentary Record.
Front. Earth Sci. 8:75.
doi: 10.3389/feart.2020.00075

Palaeomagnetic records obtained from Arctic Ocean sediments are controversial because they include numerous and anomalous geomagnetic excursions. Age models that do not rely on palaeomagnetic interpretations reveal that the majority of the changes in inclination do not concur with the established global magnetostratigraphy. Seafloor oxidation of (titano)magnetite to (titano)maghemite with self-reversal of the (titano)maghemite coatings has been proposed as an explanation. However, no existing model can explain when the self-reversed components formed and how they are linked to litho-stratigraphic changes in Arctic Ocean sediments. In this study, we present new palaeo- and rock magnetic measurements of a sediment core recovered from the Arlis Plateau, close to the East Siberian Shelf. The magnetic data set is evaluated in the context of the regional stratigraphy and downcore changes in physical and chemical properties. By cross-core correlation, we show that magnetic inclination changes in the region do not stratigraphically align, similar to results of studies of sediments from the Lomonosov Ridge and Yermak Plateau. Rock magnetic and chemical parameters indicate post-depositional diagenetic changes in the magnetic mineral assemblage that can be linked to manganese cycling in the Arctic Ocean. The potential presence of a magnetic remanence bearing manganese-iron oxide phase, which can undergo self-reversal, leads to an alternative hypothesis to primary seafloor oxidation of (titano)magnetite. This phase may form by precipitation from seawater or by changing redox conditions in the sediment column by mineral precipitation from ions dissolved in pore water. These findings highlight the need for further investigation into the magnetic mineral assemblage, its link to manganese cycling and pore water geochemistry in Arctic Ocean sediments.

Keywords: Arctic Ocean, lithostratigraphy, palaeomagnetism, mineral magnetism, diagenesis

INTRODUCTION

The magnetostratigraphy of Arctic Ocean sediments has bewildered geologists because palaeomagnetic studies yield high frequency changes in polarity (e.g., Backman et al., 2004) that do not match the established Geomagnetic Polarity Time Scale (GPTS; Cande and Kent, 1995). Early works in the Arctic Ocean interpreted the observed polarity changes

as geomagnetic reversals, with the uppermost change in inclination assigned to the Matuyama-Brunhes polarity transition (e.g., Steuerwald et al., 1968; Clark, 1970), which resulted in low sedimentation rate estimates. These low rates were later challenged by alternative dating approaches, with the conclusion that the most extreme palaeomagnetic directional changes (in inclination) were records of geomagnetic excursions during the Brunhes chron (e.g., Nowaczyk et al., 1994, 2001; Jakobsson et al., 2000; Nowaczyk and Knies, 2000; Backman et al., 2004). Sedimentation rates based on the alternative dating approaches are, however, still lower than the critical rate of ca. 10 cm/ka that models of natural remanent magnetisation (NRM) acquisition by sediments predict is necessary to record short-term polarity changes, such as geomagnetic excursions (Roberts and Winklhofer, 2004).

These difficulties in interpreting palaeomagnetic data in the Arctic led to the exclusion of magnetostratigraphy in the construction of the Arctic Coring Expedition (ACEX, IODP Expedition 302) age model for the Neogene (Backman et al., 2008). Some recent studies challenge the ACEX-based age model through U-Th ages (Hillaire-Marcel et al., 2017) and palaeomagnetic interpretations (Liu et al., 2019) that support the low-sedimentation rate scenario of Clark (1970). While some studies (e.g., Spielhagen et al., 2004) of Arctic Ocean sediments assumed inclination changes to be coeval and used them for stratigraphic correlation, more recent studies that placed inclination changes into the lithostratigraphic context of the Arctic Ocean (e.g., O'Regan et al., 2008; Wiers et al., 2019) have confirmed the abnormal nature of the palaeomagnetic record by showing that inclination changes are not stratigraphically coeval.

While the entire Arctic Ocean falls into the region of the tangent cylinder (e.g., Kono and Roberts, 2002), which could hypothetically create a very different surface expression of the geomagnetic field from the rest of the world, palaeomagnetic studies from Antarctic sediments have not uncovered evidence of unregular field behaviour within the region of the tangent cylinder (Jovane et al., 2008; Lawrence et al., 2009). Most work on post-depositional transformations of magnetic minerals in marine and lacustrine sediments has focussed on sulphide-driven iron-oxide dissolution and the authigenesis of ferrimagnetic iron sulphides (reviewed by Roberts, 2015). However, Channell and Xuan (2009) proposed that the observed changes in palaeomagnetic direction in Arctic sediments are the result of post-depositional seafloor oxidation of (titano)magnetite to (titano)maghemite. This oxidation is accompanied by the acquisition of a reversed chemical remanent magnetisation (CRM) in the (titano)maghemite phase. The process would therefore, be similar to that already proposed to explain anomalous palaeomagnetic records from the North Pacific (Kent and Lowrie, 1974; Johnson et al., 1975). Although Xuan and Channell (2010) further developed the model and showed that Arctic Ocean sediments contain a population of high-Ti magnetite with high oxidation states, which are necessary to form reversed CRM's (O'Reilly and Banerjee, 1966), a clear mechanism that differentiates normal from reversed zones is still missing. Particularly troublesome is that the observed mean Ti content (x) is less than 0.5 (Xuan and Channell, 2010), which is too low for a

reversed CRM to form (O'Reilly and Banerjee, 1966). Henshaw and Merrill (1980) proposed that a magnetic ferromanganese phase is responsible for the anomalous palaeomagnetic records from the North Pacific, which is also a conceivable scenario for Arctic sediments, amongst others.

Modern, interglacial and interstadial sediments from the central Arctic Ocean tend to be relatively fine-grained, bioturbated brown clays and silty-clays that contain, at least in near surface sediments, calcareous microfossils. The brown colour comes from a notable enrichment in the manganese (Mn) content of interglacial and interstadial sediments (Jakobsson et al., 2000). Although Mn can undergo post-burial remobilisation, bioturbated, brown (Mn-enriched) layers are widely used for the lithostratigraphic correlation and dating of Arctic marine sediments (e.g., Jakobsson et al., 2000; März et al., 2011; Löwemark et al., 2014; Schreck et al., 2018; Ye et al., 2019). Mn and Fe cycling in the sediments has received little to no attention with respect to palaeo- and rock magnetic data, even though ferromagnetic manganese minerals exist, such as jacobsite (MnFe_2O_4). Fe/Mn ratios in Arctic ferromanganese nodules are considerably higher than deposits in other ocean basins (Hein et al., 2017; Konstantinova et al., 2017, 2018) and there is a known connection between Mn and Fe redox reactions (e.g., Schulz and Zabel, 2006).

In this study we present new palaeo- and rock magnetic data in combination with physical and chemical properties of sediments from the Arlis Plateau close to the East Siberian Shelf, Arctic Ocean. These data are evaluated in the context of the regional litho- and chronostratigraphy (Schreck et al., 2018) with a focus on diagenetic changes associated with Mn cycling (März et al., 2011; Löwemark et al., 2014).

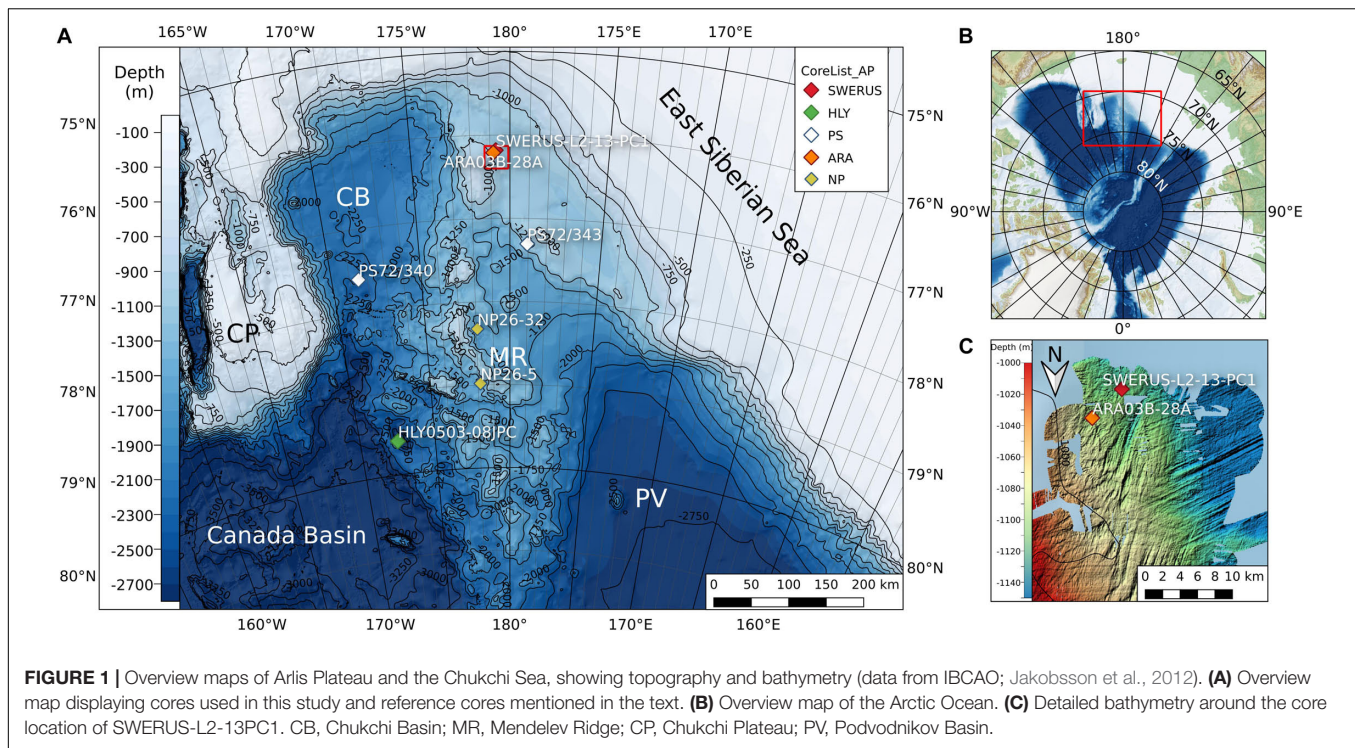
MATERIALS AND METHODS

Coring Site and Sampling

The studied piston core SWERUS-L2-13-PC1 (hereafter referred to as 13PC; **Figure 1**) was collected from the Arlis Plateau (76.18° N, 179.29° E) during the Swedish-Russian-US expedition on the Swedish icebreaker Oden in 2014, from a water depth of 1119 m. The core length was 7.68 m. Samples for organic carbon and sterols were taken onboard after splitting, with 10 cm³ scoops and frozen at -20°C. The core was stored at 4°C before the archive halves were subsampled with standard palaeomagnetic cubes (7 cm³) at Stockholm University in 2016.

Physical Properties

Bulk density (BD, ρ) and magnetic susceptibility (κ) were measured shipboard at 1 cm downcore resolution on whole core sections approximately 24 h after the core was recovered. Measurements were performed using a GeoTek multi-sensor core logger (MSCL). Line scan images were taken from the archive halves after splitting. A fall cone was used to measure the undrained shear strength of the sediment on the working halves. Sediment colour is often used in the western Arctic Ocean as an indicator for glacial-interglacial cycles and cross-core correlation (Jakobsson et al., 2000). We measured sediment colour of



the archive halves with a handheld Minolta spectrophotometer (model CM-700d) at 2 cm intervals at Stockholm University. Colours are expressed as components of lightness (L), green-red (a^*) and blue-yellow (b^*). Radiographic images were obtained from the archive halves using an ITRAX core scanner (Stockholm University) with a Mo tube at 30 kV, 45 mA and 200 μm increments.

(Organic)Geochemical Properties

Relative elemental composition was measured by means of X-Ray Fluorescence (XRF) with the ITRAX core scanner on the archive halves of the core. Measurements were made with a Mo tube (30 kV, 45 mA and 20 s dwell time) at 2 mm increments. Elements with low average counts and/or noisy signals (Al, P, S, Ga, Y, Ba, Ta, W) and elements that exhibited large concentration changes at section breaks (Ar, Ni, Pb), were disregarded. The remaining elemental counts (Si, Cl, K, Ca, Ti, V, Cr, Mn, Fe, Cu, Zn, Br, Rb, Sr, Zr) were normalised to the ratio of incoherent to coherent scattering and log normalised (base e).

Total organic carbon (TOC), the stable isotopic composition of organic carbon ($\delta^{13}\text{C}_{\text{org}}$) and sterol concentrations were measured at 10 cm resolution at the Department of Geological Sciences, Stockholm University. Samples were freeze-dried and homogenised in the laboratory before subsequent analyses. For TOC and $\delta^{13}\text{C}_{\text{org}}$, the homogenised samples were first treated with a 1M HCl-solution to remove any carbonates, and then measured using a Carlo Erba NC2500 elemental analyser coupled to a Finnigan Delta V Advantage mass spectrometer. For the sterols, Androstanol was added as an internal standard before extraction to allow quantification of the concentration of sterols in the sediments. The homogenised samples were subjected to

three cycles of 15 min sonication with dichloromethane and methanol (DCM/MeOH; 2:1 v/v), followed by centrifugation and decanting to obtain the total organic extracts. The polar fraction containing the sterols was eluted with DCM:MeOH (1:1) using glass pipette columns packed with pre-combusted silica gel and cotton wool. The fraction was silylated in BSTFA and pyridine (1:1) at 60°C for 20 min. The samples were then further separated using a Shimadzu QP2010 Ultra Gas Chromatography-Mass Spectrometry (GC-MS) with a ZB-5-HT column using a temperature increase of 10°C/minute from 40 to 300°C. The abundances of brassicasterol and β -sitosterol were quantified as trimethylsilyl ethers (TMS) in selected ion mode (SIM) at m/z 470 and m/z 486, respectively.

Magnetic Properties

Anisotropy of magnetic susceptibility (AMS) and frequency dependent magnetic susceptibility were measured with an AGICO MFK1-FA Kappabridge equipped with a sample rotator for spinning specimen measurements in three positions (Pokorný et al., 2011) at the Department of Earth Sciences, Uppsala University, Sweden. AMS was measured to assess potential sampling induced fabric deformation and identify resulting unreliable palaeomagnetic records (Marino and Ellwood, 1978). The degree of anisotropy (P_j) and the shape parameter (T ; both after Jelinek, 1981) describe the fabric. We further utilise the parameter $90-K_3\text{Inclination}$, where K_3 is the axis of minimum susceptibility, to identify disturbed/unreliable portions of the core (Hroudá and Kahan, 1991). Where this parameter is $>15^\circ$ the palaeomagnetic directional data are considered unreliable (Snowball et al., 2019). To quantify the proportion of superparamagnetic (SP) particles we calculated $\chi_{fd1,16}$ (after

Hrouda, 2011) using bulk magnetic susceptibility measurements at 976 Hz and 15616 Hz.

NRM, anhysteretic remanent magnetisation (ARM) and isothermal remanent magnetisation (IRM) were measured with a 2G Enterprises 760 superconducting rock magnetometer (SRM) at the University of Bremen, Germany. NRM was measured and subsequently demagnetised with 15 incremental alternating field (AF) demagnetisation steps from 5 to 100 mT. Characteristic remanence magnetisation (ChRM) inclination and prolate maximum angular deviation (MAD_p ; Love, 2007) were calculated by principal component analysis (PCA) in the 20 to 60 mT demagnetisation range (Kirschvink, 1980).

ARM was imparted using an AF of 100 mT and a 0.05 mT DC bias field and subsequently measured and demagnetised using the same steps as for the NRM. Susceptibility of ARM (χ_{ARM}) was calculated by normalising ARM to the bias field. IRM was first imparted with a 2.5 T field and measured as the saturation IRM (SIRM). Afterward, 20 increasing fields from 10 to 300 mT were imparted in the opposite direction as the SIRM. Based on the IRM data we calculated the average coercivity of remanence (B_{cr}) for each sample by interpolation of IRM values to a resolution of 0.1 mT, as well as the S-Ratio and Hard IRM (HIRM) at 100 and 300 mT backfields to characterise the magnetic mineralogy. The S-Ratio gives the relative concentrations of minerals with B_{cr} higher than 100 and 300 mT, whereas HIRM is the absolute magnetisation of minerals with B_{cr} higher than 100 and 300 mT (e.g., Liu et al., 2007). ARM, SIRM and HIRM were mass normalised using the cube weights, corrected for the weight of an empty cube.

To identify magnetic domain states, hysteresis properties (Coercive force, B_c ; Saturation magnetisation M_s ; Remanent magnetisation, M_r) were measured on 20 selected samples by subsampling bulk material from the palaeomagnetic cubes. Measurements were made with a Lakeshore VSM at the Ångström Laboratory, Uppsala University, Sweden. A maximum field of 1 T was used to magnetise the samples. Measurement results were processed using HystLab (Paterson et al., 2018).

Statistical Analysis

To find relationships between different parameter types that relate to (1) sediment input or (2) diagenetic changes, we calculated Pearson correlation coefficients using the pandas python library (McKinney, 2010). To correlate values that were measured at different sampling intervals, data were resampled to match the resolution of the palaeomagnetic samples using NumPy (van der Walt et al., 2011). Corresponding values for organic carbon content and sterol concentrations were linearly interpolated. XRF values were averaged across the length (2.2 cm) of palaeomagnetic cubes.

In order to differentiate sediments based on their physical, chemical, biological and magnetic properties, we employed fuzzy c-means clustering (FCM) on data matrices with the SciKit fuzzy logic toolbox for python (Warner et al., 2017). Before clustering, data were standardised using

$$z_i = \frac{x_i - \bar{X}}{s}$$

where z_i is the standardised value, x_i the original value and s the standard deviation. Data were transformed into standard normal form to eliminate different measurement units across parameters. Clustering was performed based on Euclidean distances with a fuzzy exponent chosen according to the data matrix dimensions (after Schwämmle and Jensen, 2010). The optimal number of clusters was determined based on a combination of different validation indices (Schwämmle and Jensen, 2010).

FCM was run on a combined data set of physical (ρ , κ , L , a^* , b^*), chemical (Ca, Fe, Mn) and biological (TOC, $\delta^{13}C_{org}$, brassicasterol, β -sitosterol) data (denoted SC) and rock magnetic data (denoted MC). In the following text and figures, clusters are referred to by their denomination (SC or MC), a subscript that identifies the cluster in question (1, 2, 3, etc.) and the downcore occurrence of aforementioned cluster (a, b, c, etc.).

RESULTS

Sediment Stratigraphy

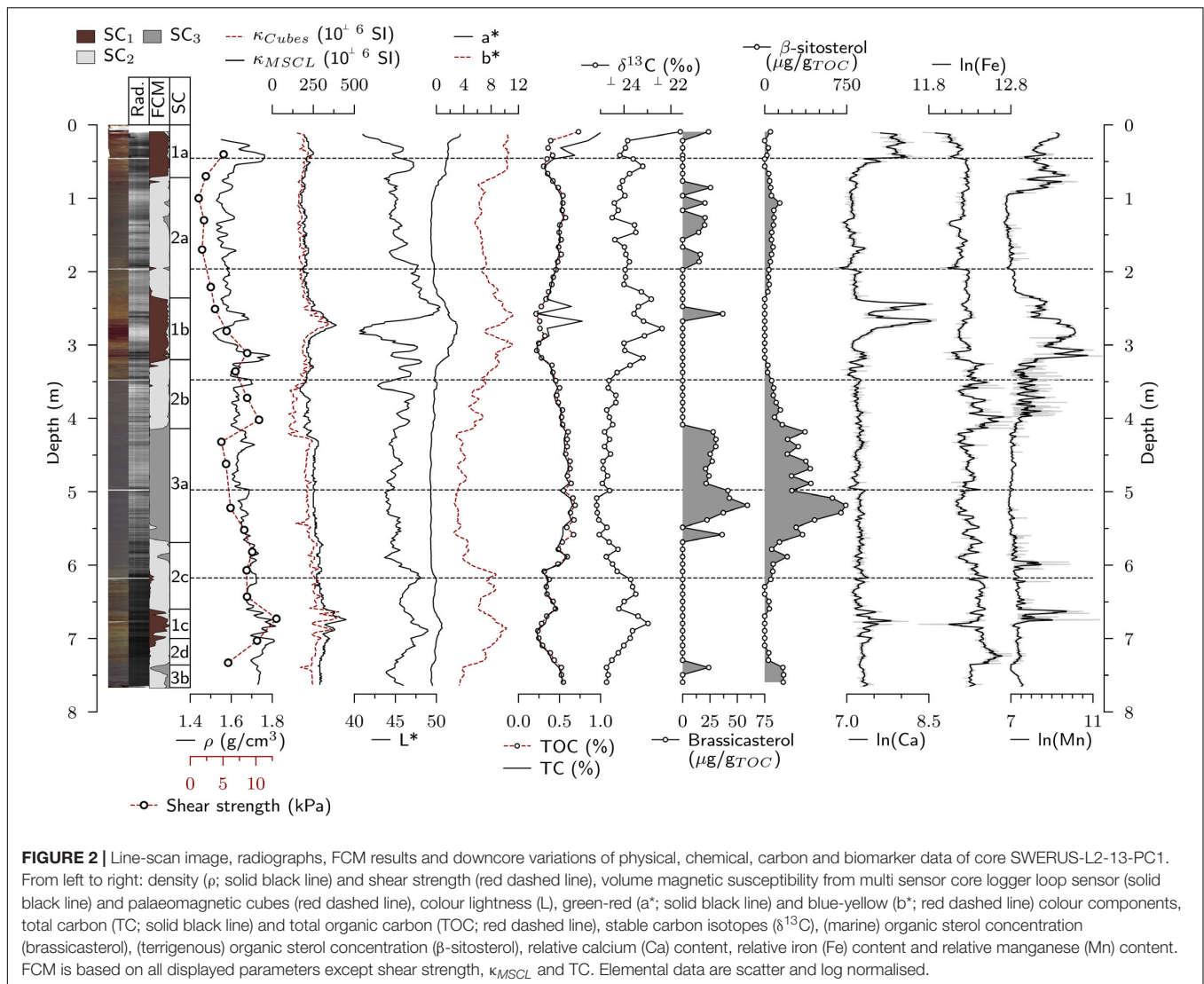
The sediments of 13PC consist of alternating dark greyish brown to olive brown (2.5Y 4/2 – 4/3) and dark grey to dark greenish grey (GLE1 4/- 4/1) layers. Density (1.5 to 1.7 g/cm³) and shear strength (~2 to 10 kPa) show a downcore trend to higher values (Figure 2), characteristic of compaction associated with dewatering as burial depth increases.

Brown layers comprise dark brown to greyish brown mud with slightly darker layers/mottles and signs of bioturbation that extend into underlying grey layers. The brown layers are characterised by red (a^*) and yellow (b^*) colour components, minimum organic carbon and sterol content, high $\delta^{13}C_{org}$ values, and high Ca and Mn. In 13PC, two distinct brown layers are found at 0 to 0.72 m and 2.5 to 3.5 m. A third layer that exhibits similar characteristics is found between 6.3 and 7.3 m. However, this third brown layer lacks high Ca concentrations, displays a larger density and lightness (L) and is a different shade of brown compared to the two other brown layers (cf., Figure 2).

Grey layers comprise olive grey to greenish grey mud with yellowish-brown layering and mottles. They display low density, low magnetic susceptibility and elevated β -sitosterol and brassicasterol concentrations. Additionally, grey layers exhibit low $\delta^{13}C_{org}$ values and low Mn and Ca concentrations.

Stability of the Natural Remanent Magnetisation

Analysis of vector end-point diagrams (Zijderveld, 1967) reveals multi component demagnetisation behaviour (Figure 3). One set of samples is characterised by the removal of a low coercivity (viscous) magnetisation between 0 and 15 mT and a more stable component of magnetisation above 15 mT. A second set of samples is characterised by a curved demagnetisation behaviour indicative of at least two components with overlapping coercivity spectra. Both sets contain normal and reversed directions. NRM averages $4.92 \times 10^{-3} \pm 3.31 \times 10^{-3}$ A/m, with slightly higher values and variability in the brown layers ($6.31 \times 10^{-3} \pm 4.12 \times 10^{-3}$ A/m) compared to the grey layers ($4.08 \times 10^{-3} \pm 2.35 \times 10^{-3}$ A/m). We attribute the shallow



inclination component found in most samples (c.f., **Figure 3**) to a viscous component acquired during horizontal storage in Stockholm between sample retrieving and sub-sampling.

The MDF_{NRM} (**Figure 4**) displays a high variability within the uppermost 2 m of the core. Below 2 m, MDF_{NRM} drops to less than 10 mT on average with high variability between 4 and 6 m. The very high values of MDF_{NRM} around 3 m are associated with low NRM intensity, which we attribute to the presence of anti-parallel directional components that have overlapping coercivities. Additionally, samples from the uppermost 2 m of the core exhibit a predominantly inverted AMS fabric as identified by the 90-K₃ parameter.

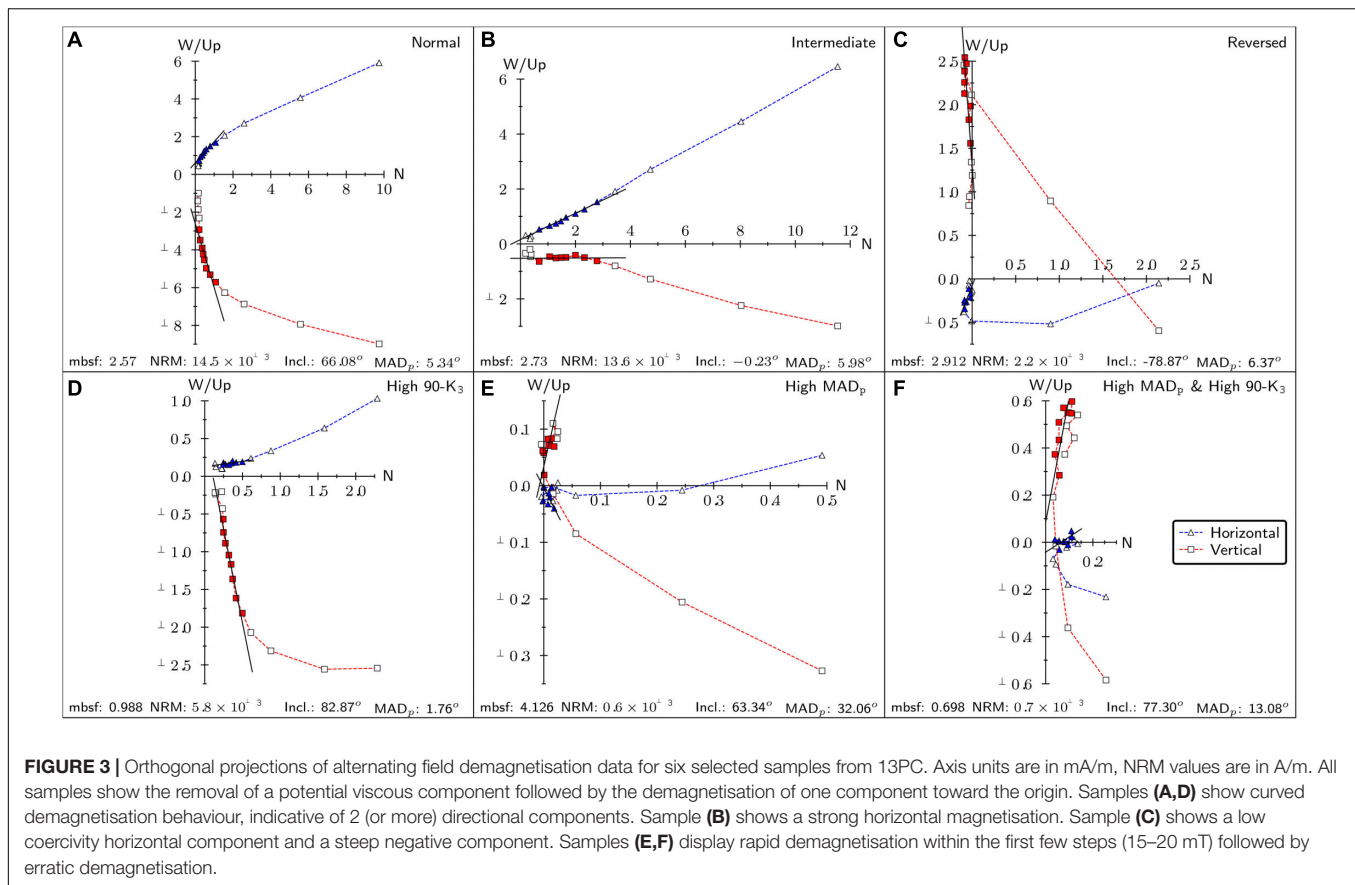
PCA isolated ChRM inclinations in the range of 20 to 60 mT show average MAD_p values of approximately 8° with 28% being steeper than 10° (**Figure 4**). Almost 20% of the samples show an inclination below 0° that is prevalent in, but not restricted to, brown layers. Using rejection criteria to filter ChRM inclination based on high MAD_p values (>10°) and the detection of potentially disturbed

sediment (90-K₃ > 15°) discards about half (149 out of 283) of the data set.

Rock Magnetic Properties

Values of χ , χ_{ARM} and SIRM suggest high concentrations of magnetic minerals in brown layers (**Figure 5**) although the most prominent peak in concentration, between 2.5 and 3.0 m, is slightly offset across the parameters. The peak in χ_{ARM} is approximately 0.1 m deeper than in χ and SIRM, although the peak in χ_{ARM} coincides with a peak in χ_{fd} . The HIRM reveals that magnetic minerals with coercivities > 100 mT but lower than 300 mT are more prominent in the uppermost 4.25 m of the core. Accordingly, magnetic mineralogical dependent parameters (S-Ratio, B_{cr}) indicate a distinct change to a lower average coercivity at 4.25 m. This change is accompanied by an increase in degree of anisotropy (P_j) and shape (T) of the magnetic susceptibility ellipsoid below 4.25 m.

The ratios of ARM/SIRM, χ_{ARM}/χ and SIRM/ κ , which are commonly interpreted as proxies for magnetic domain



state or magnetic mineralogy (Peters and Dekkers, 2003) are dominated by magnetic mineralogy changes in 13PC (Figure 6A). The peaks at 0.15 and 2.8 m in ARM/SIRM and χ_{ARM}/χ coincide with peaks in χ_{ARM} and SIRM and lows in B_{cr} and S-Ratio₁₀₀ (Figure 5), which indicates a higher concentration of low coercivity magnetic minerals rather than changes in magnetic domain state of a single mineral. Accordingly, SIRM/ χ follows trends in SIRM, S-Ratio₁₀₀ and HIRM₁₀₀, which indicates a strong influence of compositional changes in the magnetic mineral assemblage. Results from hysteresis measurements (Figure 6B) confirm this influence by showing a low correlation of B_{cr}/B_c vs. M_{rs}/M_s values with χ_{ARM}/χ . The interpretation of the Day plot (Figure 6; Day et al., 1977) is, however, complex because the magnetic hysteresis parameters are influenced by a large number of factors, such as mineralogy, magnetocrystalline anisotropy and particle interactions to name just three (Roberts et al., 2018).

Statistics

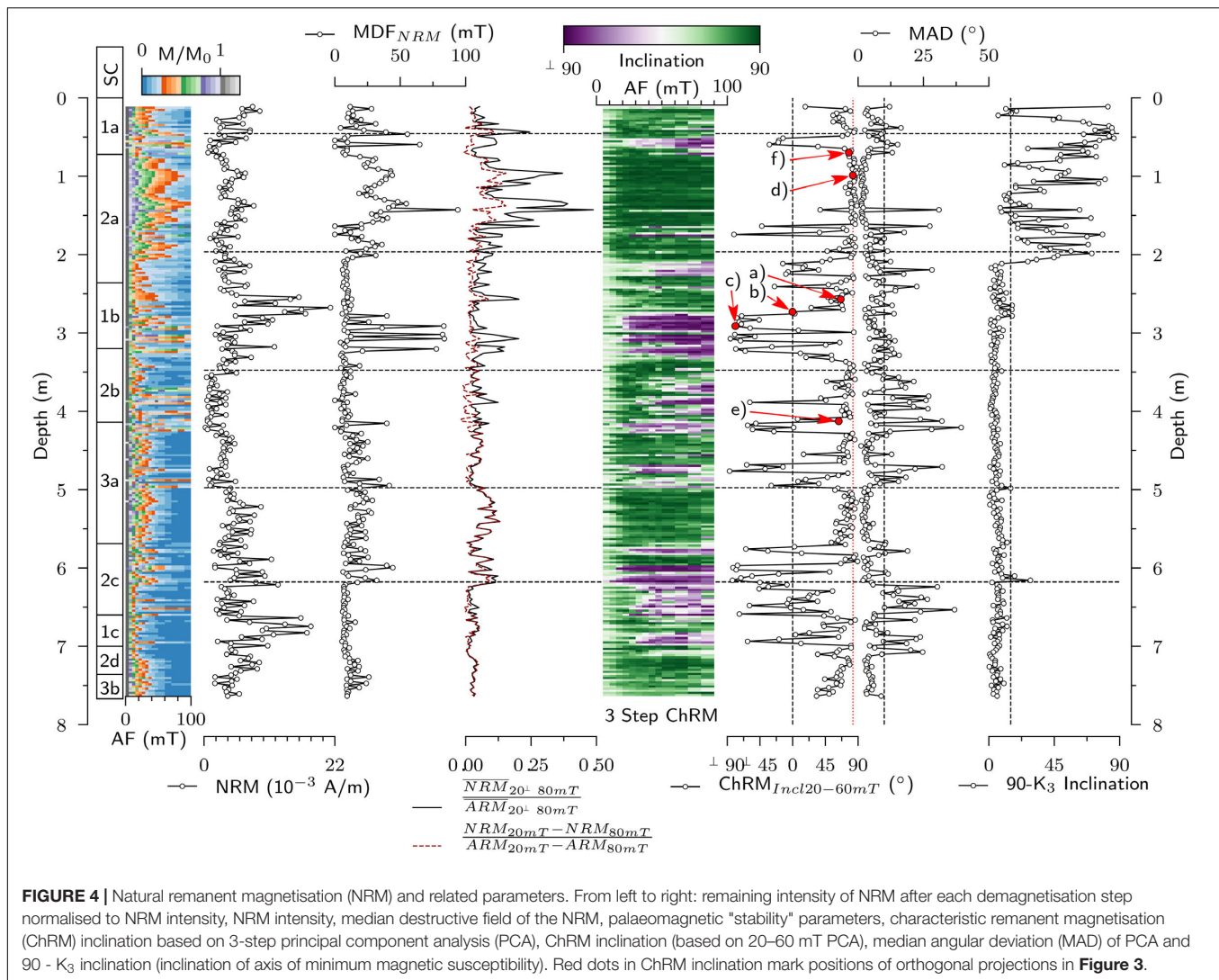
The optimal number of clusters was determined to be 3 for both FCM runs (SC and MC) with a fuzzy exponent of ~ 1.3 . Results from SC confirm our initial division into brown and grey layers with SC₁ correlating with brown layers while SC₂ and SC₃ correlate with grey layers (Figure 2). The subdivision of the grey layers in the FCM results is mainly based on differences in β -sitosterol, brassicasterol and Mn concentrations.

MC results indicate that there is no simple connection between magnetic properties of 13PC and its other physical and chemical properties (Figure 5). Based on its magnetic properties, the core can clearly be divided into an upper part (0–4.25 m, MC₁ and MC₂) and a lower part (4.25 m and below, MC₃) that display different magnetic properties. The division is mainly based on the difference in high coercivity minerals (i.e., >100 mT, based on S-Ratio₁₀₀) because a clear separation is not apparent in FCM results from physical and chemical properties (i.e., the SC clusters). MC₁ is characterised by high values in χ , χ_{fd} , χ_{ARM} , SIRM and HIRM₁₀₀ while MC₂ and MC₃ are characterised by lower values in χ_{fd} and χ_{ARM} . MC₂ and MC₃ are distinctly different in their χ , SIRM, HIRM₁₀₀, S-Ratio₁₀₀ and B_{CR} values. SC and MC correlate within the first 4 m of 13PC, but with offsets in the location of boundaries. MC₁ correlates with SC₁ but is thinner, whereas MC₂ and MC₃ are not uniquely bound to SC₂ and SC₃ but merely separate the core into an upper and lower part.

DISCUSSION

Stratigraphy and Age Constraints

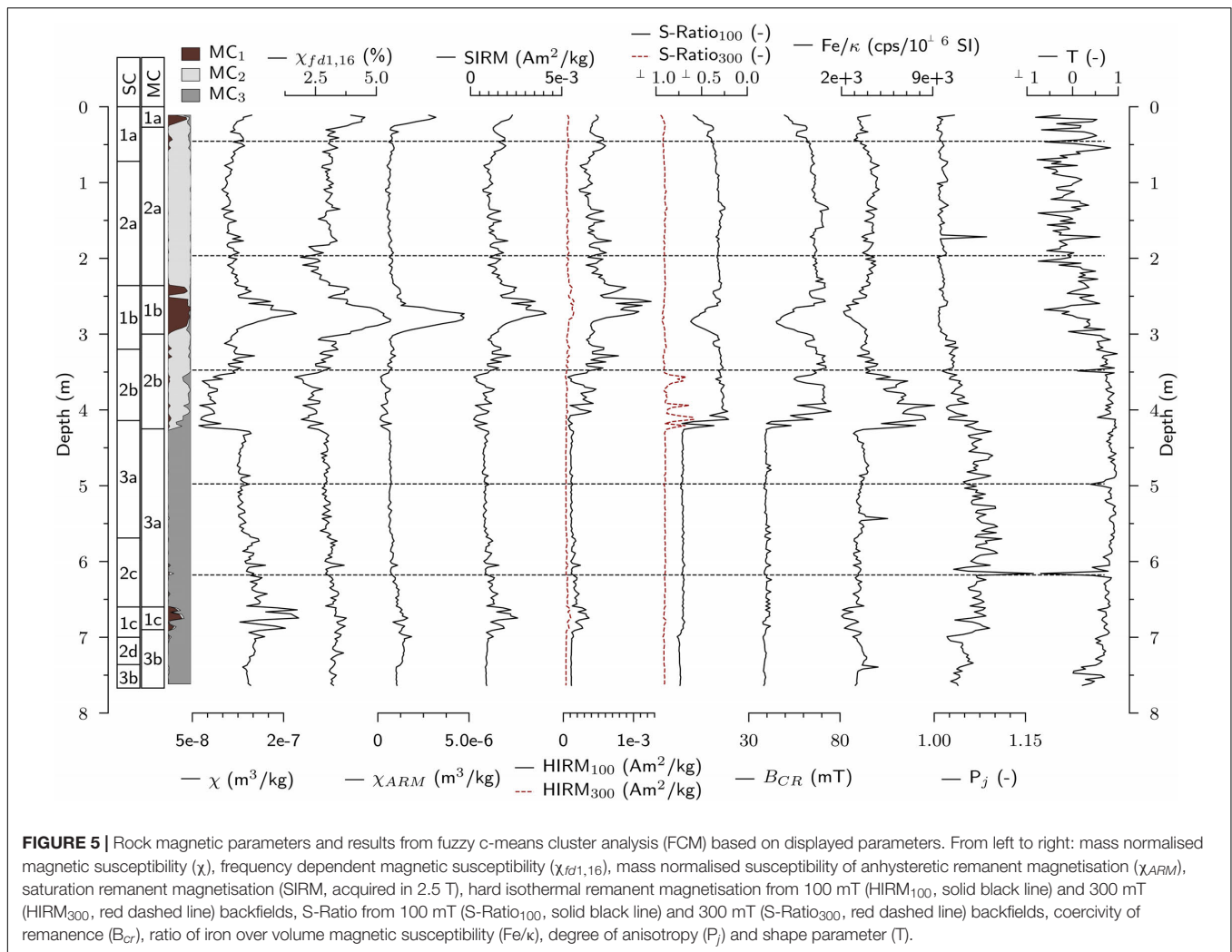
The lithostratigraphy of core 13PC is similar to other cores from the region, specifically nearby cores ARA03-28A and HLY0503-8JPC (hereafter 8JPC; Adler et al., 2009; Schreck et al., 2018;



Figures 7, 8). The lithostratigraphic framework presented by Schreck et al. (2018) follows the nomenclature used in the western Arctic with dark brown layers labelled as Bx and yellowish to greyish layers labelled Gx, where x is a downcore increasing number that indexes the occurrence of successive layers. The dark brown layers are interpreted to represent interglacial intervals while the grey layers represent glacial intervals. We find a good correlation of brown layers B1 and B2 in 13PC and ARA03-28A, with the characteristic double peak in Ca in layer B2 (**Figure 7**). Three radiocarbon ages from core 13PC (**Table 1**; Jakobsson et al., 2016) confirm a Holocene age for layer B1 and a minimum MIS 3 age for B2. Jakobsson et al. (2016) further suggest an MIS 5 age for B2 based on the rare occurrences of *E. huxleyi* and *Gephyrocapsa* spp. at 2.86 m. However, based on the stratigraphic correlation an MIS 3 age of B2 would be more consistent with reported basal ages of 40 to 45 ka for this layer (Schreck et al., 2018). The much older ^{14}C ages we obtain from our two samples from B2 (>43 and >48 ka) may be a result of reworking of older

material and a small sample size, which can bias the results toward older ages (Lougheed et al., 2018). There still remains considerable uncertainty in age-depth models for Arctic Ocean sediments, and beyond the limit of radiocarbon dating it becomes difficult to differentiate between substages in glacial cycles, or define the boundaries between glacial and interglacial marine isotope stages. Here we simply acknowledge the difference in the age models reported by Jakobsson et al. (2016) and Schreck et al. (2018), and do not present any new data to support or refute either one.

FCM results confirm the general division in brown and grey layers but they do allow for a more detailed distinction of the sediment sequence. While cluster SC₁ is closely associated with the interglacial brown layers (B1 and B2), SC₂ and SC₃ differentiate the glacial layers (G1 and G2). The differences between SC₂ and SC₃ can indicate changing depositional environments and different (glacial) conditions or they may be the result of diagenetic alterations and dewatering due to compaction. SC_{1c} shows a distinctly different colour compared



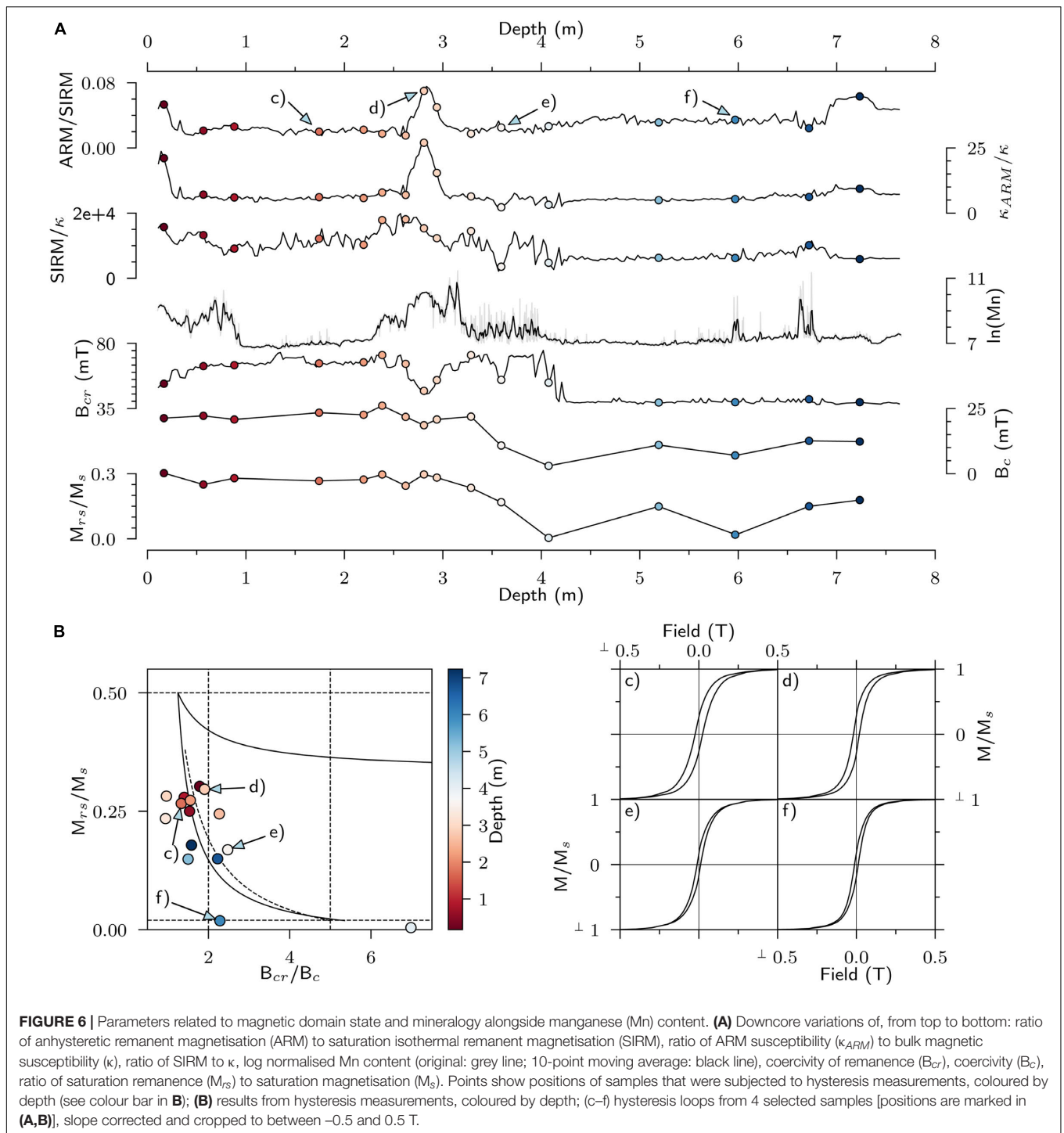
to the rest of layer G2 and may represent glacially reworked (brown) sediments as suggested by Schreck et al. (2018) for core PS72/342-1. Alternatively, SC_{1c} could represent diagenetically altered sediments as proposed by März et al. (2012) which would open the possibility that it is layer B3.

(Organic)Geochemistry

The higher (organic) carbon concentrations in the glacial or stadial grey layers in 13PC contrast with Polyak et al.'s (2004) results for cores from the Mendeleev Ridge, where more organic carbon is found in interglacial sediments (NP26 cores; Figure 1). Increased erosion and remobilisation of sediments and permafrost carbon from the Siberian Shelf during glacial or deglacial periods can explain the high values in the glacial and stadial sediments in 13PC (Martens et al., 2018). The proximity of 13PC to the shelf and the stable carbon isotope signature support this interpretation. The intervals of increased TOC and sterol concentrations are characterised by more depleted stable isotopic composition of the organic carbon, which suggests a terrestrial source (Goñi et al., 2005). While brassicasterol and β -sitosterol can have both terrigenous or marine origins, brassicasterol is

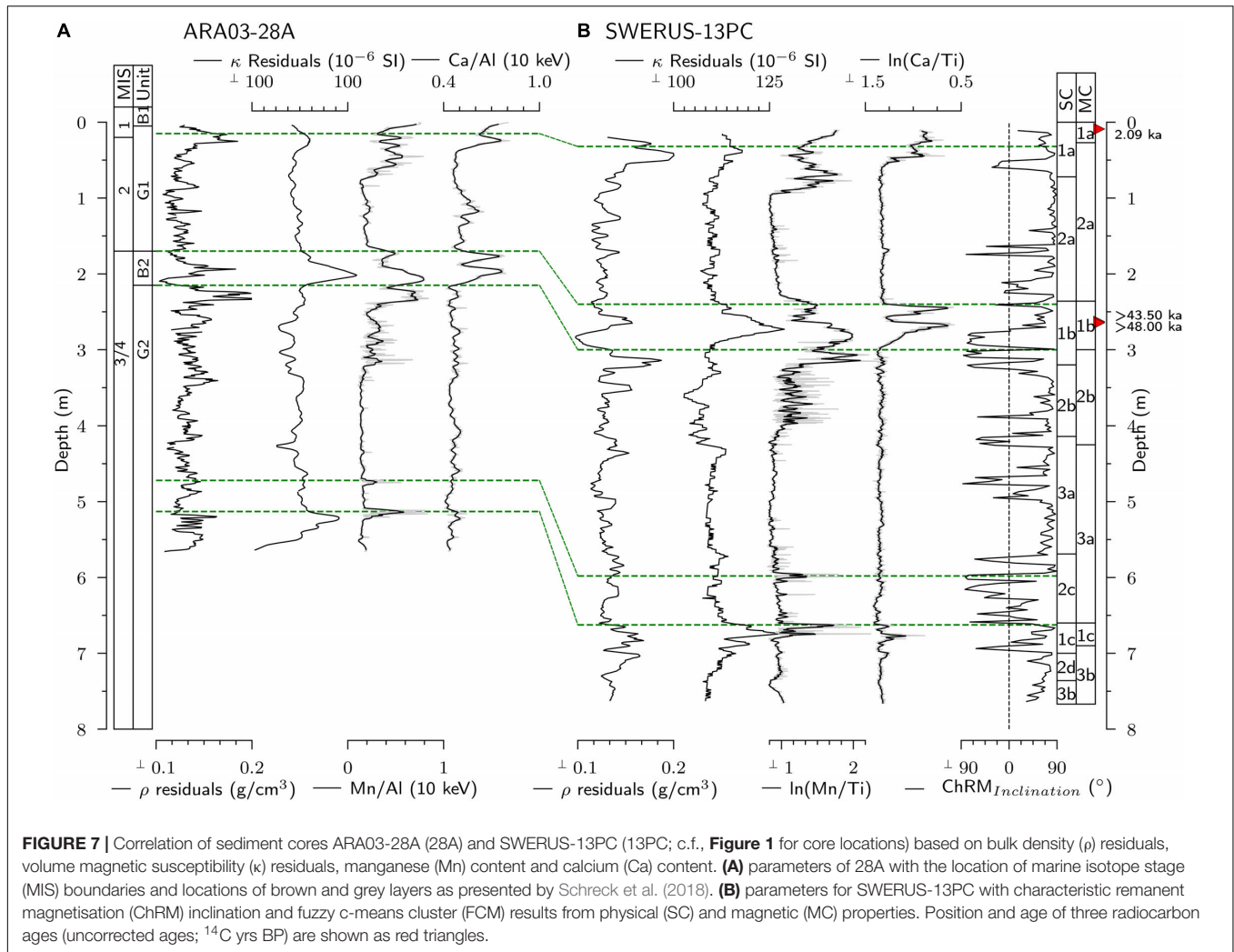
more often considered to be of marine origin whereas β -sitosterol is considered to be of terrigenous origin (Fahl and Stein, 2012). Further support for our interpretation is the $\delta^{13}C$ composition of the organic matter, where lower values (-24 to -25‰) are typically indicative of land-derived carbon, while pure marine organic carbon displays higher values (-21 to -22‰). The low concentrations of organic carbon in the brown layers can also be the result of immediate seafloor consumption of dominantly marine organic matter and release of carbon (as carbon dioxide) due to high microbial activity, which can be linked to increased Mn input (Löwemark et al., 2014).

High Mn concentrations in brown layers in 13PC indicate oxic bottom water conditions (Calvert and Pedersen, 1993, 1996), but we can not infer anoxic or suboxic conditions during the deposition of grey layers. It has been shown that sediment Mn content in the Arctic Ocean is controlled by variable input of Mn that correlates with glacial/interglacial cycles and that bottom waters remained oxic during glacial times (e.g., Löwemark et al., 2014). Elevated concentrations of Mn in pore waters in Arctic Ocean cores show that buried Mn rich layers undergo diagenesis (Meinhardt et al., 2016). Mn (oxyhydr)oxides are



dissolved under suboxic conditions and dissolved Mn migrates upwards to reprecipitate in oxic pore waters. The effect of this process is clearly seen within some of the late Quaternary diamicts identified in sediment cores on the central Lomonosov Ridge. Decimeter scale intervals within these diamicts are dark grey, contain higher concentrations of TOC than surrounding interglacial sediments, with unusual spikes in Mn concentration

found at the top and/or base of these intervals (see **Figure 4** in Löwemark et al., 2014). The lowermost brown layer in 13PC, classified as SC_{1c}, may thus be layer B3 that underwent extensive Mn reduction. Mn variations have been used in the Arctic Ocean for cross-core correlation and cyclostratigraphy (Jakobsson et al., 2000; Ye et al., 2019; Park et al., 2020), however, the possibility of asynchronous Mn diagenesis in some areas and downcore



intervals necessitates considerable scrutiny before using the approach (März et al., 2011; Meinhardt et al., 2016).

Palaeomagnetism

Correlative patterns in downcore inclination changes in Arctic Ocean sediments, whether they are a genuine palaeomagnetic field recording or a diagenetic chemical remanence, are often assumed as evidence of synchronicity (e.g., Frederichs, 1995; Jakobsson et al., 2001; Adler et al., 2009; Polyak et al., 2009). However, when cores are aligned using independent lithological parameters it becomes clear that inclination changes fall within different intervals (O'Regan et al., 2008; Wiers et al., 2019).

The changes in inclination (based on ChRM, 20–60 mT) in core 13PC are difficult to correlate to known geomagnetic field changes in the time frame provided by our (litho)stratigraphic correlation. Some excursions coincide with globally accepted geomagnetic excursions, e.g., the negative inclination interval at approximately 3 m which dates at around 40 ka (i.e., the age of the Laschamps excursion). On the other hand, given the frequent occurrence of anomalous palaeomagnetic directions in sediments that were probably deposited during

periods when no accepted excursions took place, we cannot rule out that apparently genuine features simply coincide with accepted excursions.

Channell and Xuan (2009) and Xuan and Channell (2010) proposed that negative inclinations are carried by a reversed CRM caused by seafloor oxidation of (titano)magnetite to (titano)magnetite, similar to the explanation proposed for organic-poor pelagic sediments in the north Pacific (Kent and Lowrie, 1974; Johnson et al., 1975). However, according to O'Reilly and Banerjee (1966) Ti-content and oxidation state in titanomagnetite need to be large (e.g., for $x = 0.7$, $z > 0.8$) to generate reversed CRM's.

By placing 13PC into the stratigraphic framework of Schreck et al. (2018) (cf., **Figure 7**) we can compare it with core 8JPC (**Figure 8**; Adler et al., 2009; Schreck et al., 2018), one of the cores studied by Xuan and Channell (2010). Here we base core-to-core correlation on sediment physical and geochemical properties, not on the palaeomagnetic inclination records. In comparing 13PC and 8JPC it is evident that 13PC contains many inclination changes in a depth interval that exhibits mostly normal inclinations in the corresponding interval in 8JPC. This

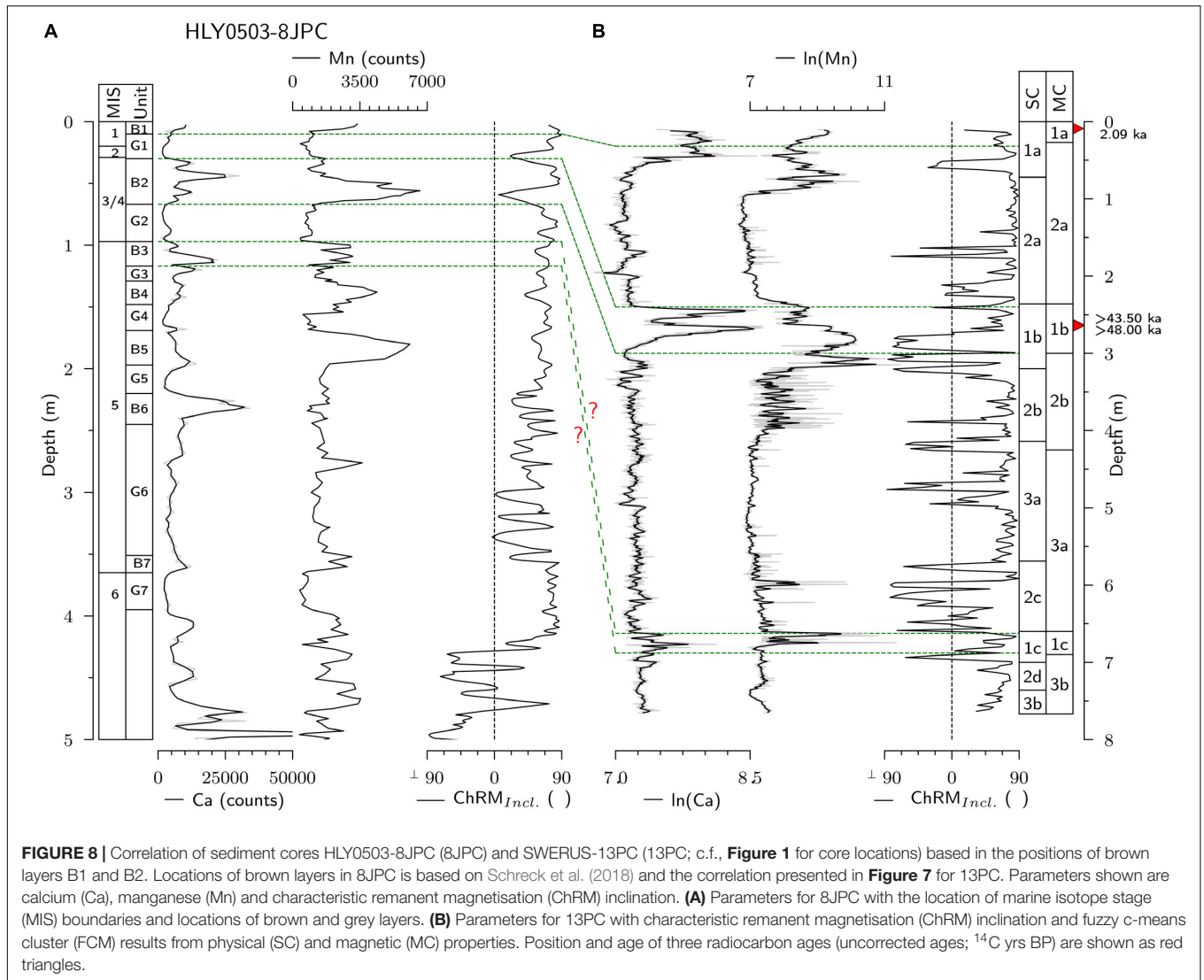


TABLE 1 | Radiocarbon ages for 13PC.

Depth (m)	Cal. Curve	Uncorrected age (14C years BP)	Calibrated age (years BP)	Source
0.09	Marine13	2090 ± 30	1175 ± 109	N. pachyderma
	IntCal13		1512.5 ± 112.5	
2.63		>43500		N. pachyderma
2.645		>48000		N. pachyderma

is an important observation, as the two cores should show a more coherent pattern if widespread seafloor oxidation, caused by low (organic) carbon influx and low sedimentation rates, is the common cause of the inclination changes. Based on the available age estimates, 13PC exhibits higher sedimentation rates than 8JPC but more intervals of negative inclination. The differences in the Ti content and oxidation state of (titano)magnetite between the two cores may explain the incoherency. However, high sedimentation rates in 13PC should reduce the exposure time of (titano)magnetite to oxic bottom waters and hence should

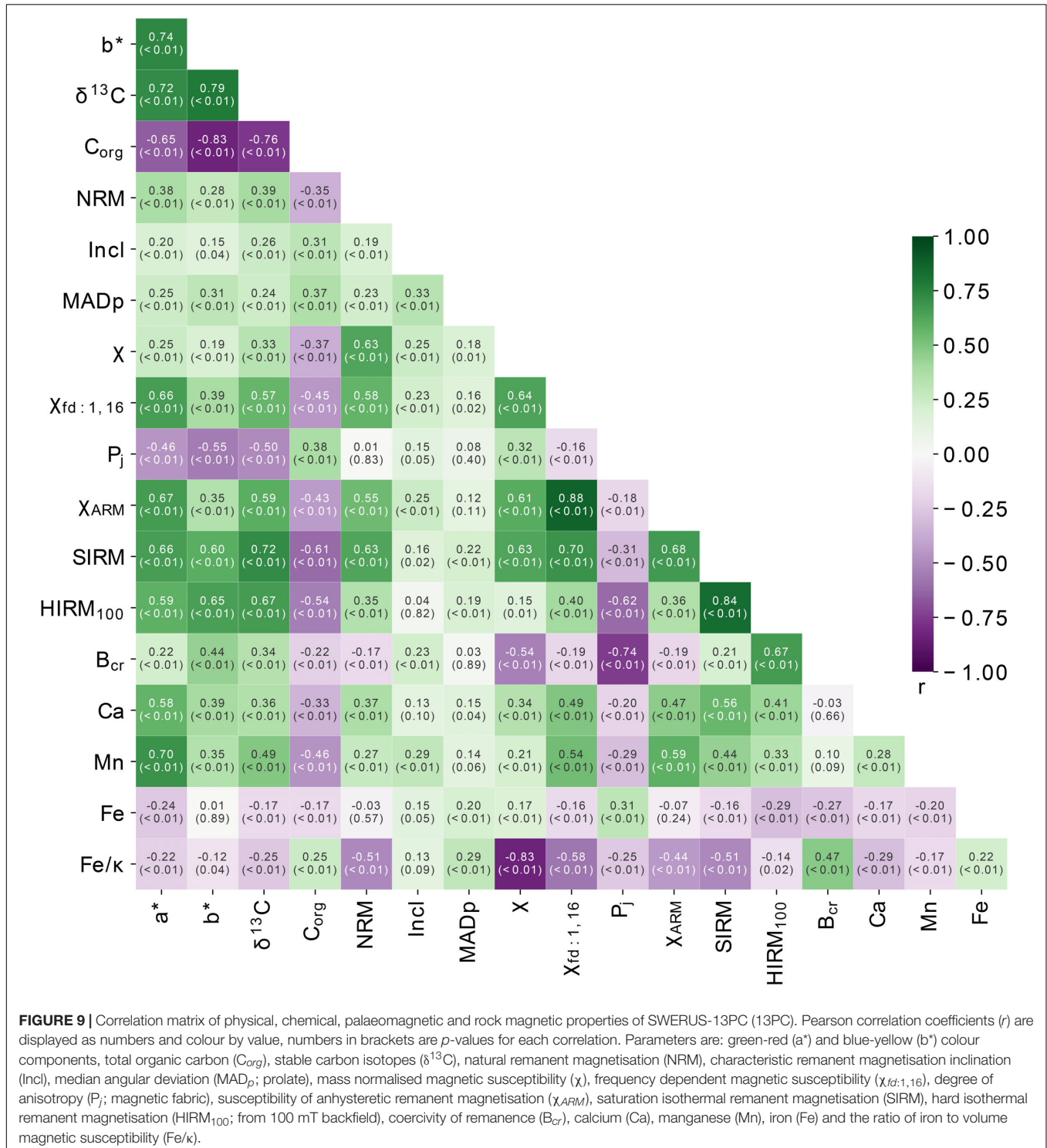
lead to a lower degree of oxidation. Additional complications arise from the fact that 8JPC's record was generated using measurements of u-channels, which smooths the signal.

Rock Magnetism

Based on FCM results on rock magnetic parameters (MC), the magnetic properties of 13PC seem to deviate somewhat from lithological changes (SC), especially below 4.15 m, which is due to the lower concentration of minerals with B_{cr} of 100–300 mT. The shift in magnetic properties may reflect a subtle diagenetic

process, since there is no comparable prominent feature in the lithostratigraphy (Figure 2). The sharp increase in Fe/k just above 4.15 m (Figure 5) is indicative of (titano)magnetite dissolution (Funk et al., 2003; Korff et al., 2016) and may mark the current or a former Fe-Redox boundary. Changes in Fe/k between 4.15 and 3.0 m are concurrent with minima in χ , χ_{ARM}

and a downcore decrease in high coercivity magnetic minerals (HIRM₁₀₀). Above the indicated dissolution front, we find a correlation of $\chi_{fd1,16}$ ($r = 0.54$; Figure 9) and χ_{ARM} ($r = 0.59$; Figure 9) with Mn that may be the result of iron (oxyhydr)oxide enrichment within a narrow band in brown layers SC_{1a} and SC_{1b} (MC_{1b}) and potentially to a lesser extent in layer SC_{1c} (MC_{1c}).



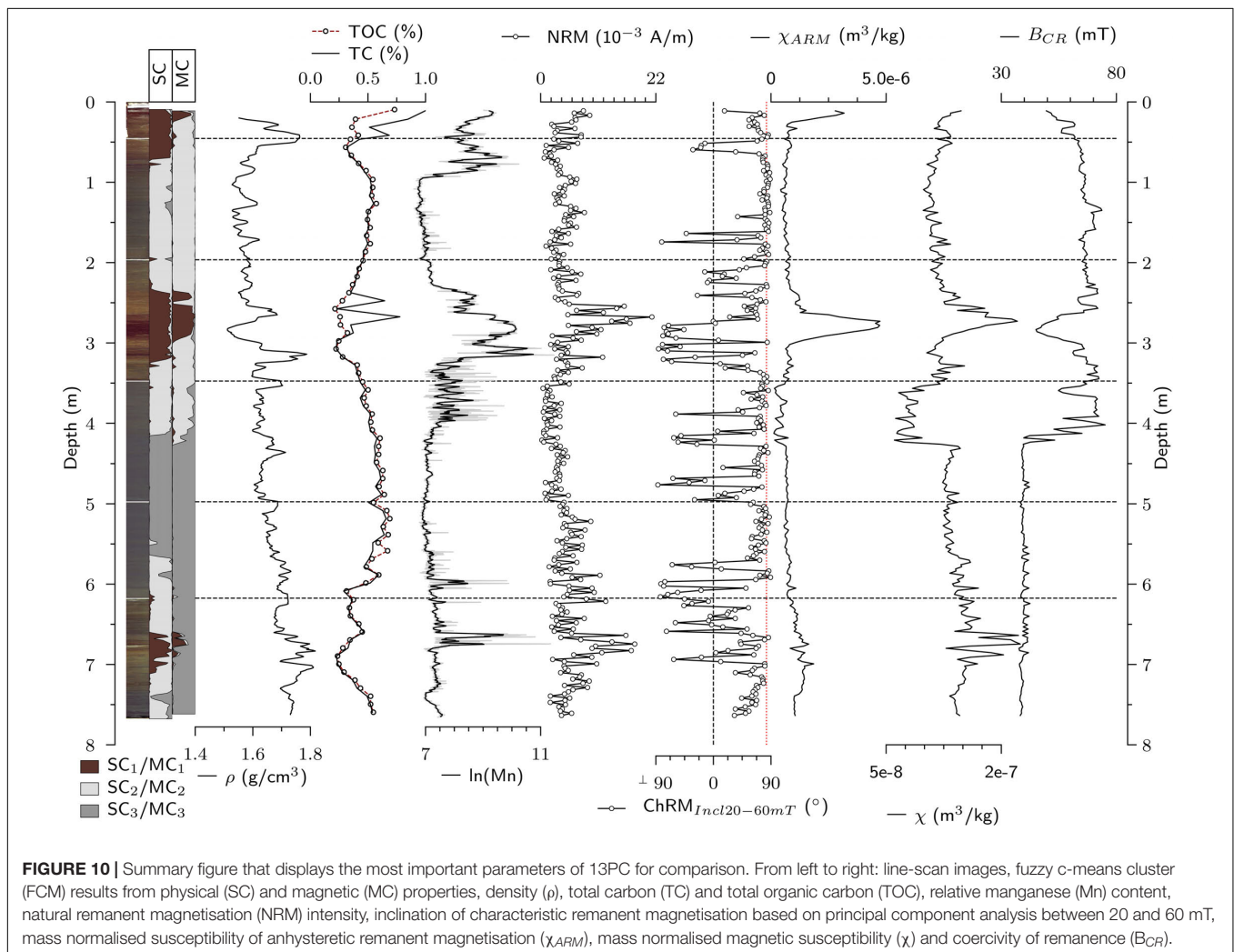
This enrichment may be facilitated by the upward migration of released iron from the underlying dissolution front (Myers and Neelson, 1988; **Figure 6**). The strong correlation of $\chi_{fd1,16}$ and χ_{ARM} ($r = 0.88$; **Figure 9**) supports the interpretation of mineral authigenesis within the sediment column.

The low concentration of high coercivity minerals below 4.15 m may be due to dissolution of one or more diagenetic-authigenic magnetic phases. Given previous work on Arctic Ocean sediments (Channell and Xuan, 2009; Xuan and Channell, 2010), a potential candidate for this phase may be coatings of (titano)magnetite that formed during seafloor oxidation. Smirnov and Tarduno (2000) show that pelagic sediments from the western equatorial Pacific contain (titano)magnetite coated in (titano)magnetite, and the coating is dissolved below the Fe-Redox boundary. The changes in hysteresis parameters Smirnov and Tarduno (2000) show are comparable to the ones in 13PC (**Figure 6**). The migration of redox fronts due to changing organic matter and Mn input across glacial-interglacial cycles (März et al., 2012) may facilitate dissolution of previously precipitated or deposited iron minerals and upward migration of released iron. To test this hypothesis, pore water ion concentration of Mn

and Fe are necessary, which do not exist for 13PC. Mn pore water concentrations from nearby core PS72/343-1 (**Figure 1**) rise below B3 or approximately 3 m, and display the reduction of Mn (oxyhydr)oxides below this depth (März et al., 2011).

Integrating Magnetic and Chemical Changes

Henshaw and Merrill (1980) showed that the anomalous palaeomagnetic record in the north Pacific is more likely due to the formation of an authigenic ferromanganese phase than to magnetisation. Substitution of Mn into the spinel lattice of (titano)magnetite can lead to self-reversals (Henshaw and Merrill, 1980), although this mechanism has not received much attention. In the Arctic Ocean, the enhanced deposition of Mn-oxides and enrichment of trace metals during interglacials shifts the Mn-Redox boundary upwards, close to the sediment/water interface. This shift triggers Mn cycling (März et al., 2011) and associated enrichment of iron (oxyhydr)oxides (Fe_{ox1} and Fe_{ox2} in März et al., 2012). Reduced Mn input during glacials results in potential diagenetic Mn redistribution in deeper sediment layers



that may lead to post-depositional biogeochemical Fe cycling and (titano)magnetite/maghemite formation (März et al., 2012).

März et al. (2012) did not find a direct relationship between Fe_{mag} [(titano)magnetite, (titano)maghemite] and χ , hinting at a different magnetic carrier in the Mn-rich (brown) layers. Similarly, in 13PC Mn shows weak to zero correlation with magnetic susceptibility ($r = 0.21$; **Figure 9**) even though Mn has been shown to be linked to iron reduction (Myers and Neelson, 1988; Smirnov and Tarduno, 2000). The precipitation of ferromanganese oxides, congruent to what was proposed for north Pacific sediments (Henshaw and Merrill, 1980), is conceivable in the Arctic Ocean. The formation of these oxides would be linked to Mn influx and changing redox conditions (**Figure 6**) and may present an alternative hypothesis to seafloor oxidation or genuine recordings of the palaeomagnetic field, and would explain the unusual palaeomagnetic record in 13PC. März et al. (2012) used the same extraction method for the Fe_{ox1} phase as Henshaw and Merrill (1980) used to dissolve a magnetic manganese-iron phase. The Fe_{ox1} phase could, therefore, contain an unidentified magnetic ferromanganese phase and the correlation of Fe_{ox1} to Mn content found by März et al. (2012) supports our hypothesis of a link between the anomalous palaeomagnetic records and the presence of ferromanganese oxides.

Neither lithology nor magnetic mineral composition show a strong correlation to the ChRM inclination. On the other hand, there is a weak correlation between ChRM inclination and Mn ($r = -0.29$; **Figure 9**). As expected, NRM intensity is more strongly affected by changes in the composition of the magnetic mineral assemblage (SIRM - NRM, $r = 0.64$; χ - NRM, $r = 0.61$; χ_{ARM} - NRM, $r = 0.58$; **Figure 9**). The low correlation coefficient between Mn and ChRM inclination may be a result of the dominantly bimodal nature of the inclination data and ongoing processes driving Mn redistribution within the sediments. A more robust approach to test the correlation was applied by calculating the circular-linear correlation coefficient (e.g., Mardia and Jupp, 2009), however, this results in the same coefficient ($r = -0.29$) for Mn and ChRM inclination. Yet, correlation of the filtered ChRM inclination with Mn yields a larger coefficient ($r = -0.47$). On the other hand, visual inspection of Mn and ChRM inclination reveals some coherence between negative inclinations and increased Mn values (**Figure 10**).

Non-steady-state diagenesis (Kasten et al., 2004), driven by changes in sediment input and bottom water ventilation, may facilitate upward migration of released ions that further distort the magnetic record. Changes in sea level across interglacial/glacial cycles that move the position of (Arctic) Atlantic water may also impact the position of redox boundaries, especially in water depths of <1500 m where the lower boundary of the Atlantic water layer generally resides today (Rudels, 2009).

CONCLUSION

Sediment core 13PC from the Arlis Plateau, western Arctic Ocean, displays a perplexing palaeomagnetic record that is

common to many Arctic Ocean sediment cores. By integrating 13PC into the regional lithostratigraphy, we are able to show that magnetic inclination changes were not recorded synchronously across the region. This finding means that one should not use inclination changes in Arctic Ocean sediments as magnetostratigraphic tie points because there is no common primary, regional lithological control over the palaeomagnetic record. Our combined magnetic and chemical approach suggest that seafloor oxidation of (titano)magnetite to (titano)maghemite takes place as proposed for other cores from the western Arctic Ocean (Channell and Xuan, 2009; Xuan and Channell, 2010). However, deeper diagenetic changes that are linked to Mn-oxide and Fe-oxide reduction may completely or partially remove (titano)maghemite coatings formed by seafloor oxidation. This challenges the ubiquitous role of seafloor oxidation as a mechanism for reversed palaeomagnetic inclinations in Arctic Ocean sediments. Our study suggests that the palaeomagnetically important diagenetic changes take place between 3 and 4 meters below the seafloor. The main lines of evidence are (1) changes in the magnetic mineral assemblage in the form of the absence of a > 100 mT (but <300 mT) magnetic mineral component, (2) changes in the magnetic fabric and (3) the identification of a (titano)magnetite/(titano)maghemite dissolution zone by Fe/ κ . Peaks in magnetic parameters (χ , χ_{ARM} , SIRM) display an increased concentration of a fine-grained (high $\chi_{fd1,16}$) magnetic phase within Mn-rich brown layers in 13PC. These measurements point to the precipitation of authigenic magnetic ferromanganese minerals and hence the acquisition of a secondary CRM that may be superimposed upon (and partially replace) a primary NRM. This process potentially occurs in addition to seafloor oxidation of (titano)magnetite to (titano)maghemite or may even be facilitated by initial oxidation. The position of high χ_{ARM} , high Mn layers suggests a link between magnetic mineral diagenesis and glacial/interglacial cycles as expressed by enhanced Mn precipitation during interglacials.

To summarise, our study of Arctic Ocean sediments leads us to hypothesise that there is a connection between the Arctic Mn-cycle and magnetic mineral diagenesis, which leads to the perplexing palaeomagnetic record. The hypothesis can be tested through a thorough investigation of (1) chemical changes related to diagenetic redox horizons, solid phase (mineralogy of magnetic minerals) and pore water measurements, combined with (2) palaeomagnetic and rock magnetic investigations.

DATA AVAILABILITY STATEMENT

The data are available on PANGAEA (<https://www.pangaea.de/>, keyword: SWERUS-C3).

AUTHOR CONTRIBUTIONS

SW, IS, MO'R, and BA developed the concept for the manuscript. MO'R was involved in the organisation and implementation of the icebreaker led expedition that

- Konstantinova, N., Hein, J. R., Gartman, A., Mizell, K., Barrulas, P., Cherkashov, G., et al. (2018). Mineral phase-element associations based on sequential leaching of ferromanganese crusts, amerasia basin arctic ocean. *Minerals* 8:460. doi: 10.3390/min8100460
- Korff, L., Dobeneck, T. V., Frederichs, T., Kasten, S., Kuhn, G., Gersonde, R., et al. (2016). Cyclic magnetite dissolution in Pleistocene sediments of the abyssal Northwest Pacific Ocean: evidence for glacial oxygen depletion and carbon trapping. *Paleoceanography* 31, 600–624. doi: 10.1002/2015pa002882
- Lawrence, K. P., Tauxe, L., Staudigel, H., Constable, C. G., Koppers, A., McIntosh, W., et al. (2009). Paleomagnetic field properties at high southern latitude. *Geochem. Geophys. Geosystems* 10, 1–27. doi: 10.1029/2008gc002072
- Liu, J., Shi, X., Liu, Y., Liu, Q., Liu, Y., Zhang, Q., et al. (2019). A thick negative polarity anomaly in a sediment core from the central arctic ocean: geomagnetic excursion versus reversal. *J. Geophys. Res. Solid Earth* 124, 10687–10703. doi: 10.1029/2019JB018073
- Liu, Q., Roberts, A. P., Torrent, J., Horng, C.-S., and Larrasoana, J. C. (2007). What do the HIRM and S-ratio really measure in environmental magnetism? *Geochem. Geophys. Geosyst.* 8, 1–10. doi: 10.1029/2007gc001717
- Lougheed, B. C., Metcalfe, B., Ninnemann, U. S., and Wacker, L. (2018). Moving beyond the age–depth model paradigm in deep-sea palaeoclimate archives: dual radiocarbon and stable isotope analysis on single foraminifera. *Climate Past* 14, 515–526. doi: 10.5194/cp-14-515-2018
- Love, J. J. (2007). “Principal component analysis in paleomagnetism,” in *Encyclopedia of Geomagnetism and Paleomagnetism*, eds D. Gubbins and E. Herrero-Bervera (Dordrecht: Springer), 845–850. doi: 10.1007/978-1-4020-4423-6_271
- Löwemark, L., März, C., O’Regan, M., and Gyllencreutz, R. (2014). Arctic ocean mn-stratigraphy: genesis, synthesis and inter-basin correlation. *Quat. Sci. Rev.* 92, 97–111. doi: 10.1016/j.quascirev.2013.11.018
- Mardia, K. V., and Jupp, P. E. (2009). *Directional Statistics*. Hoboken, NJ: John Wiley & Sons.
- Marino, R. J., and Ellwood, B. B. (1978). Anomalous magnetic fabric in sediments which record an apparent geomagnetic field excursion. *Nature* 274, 581–582. doi: 10.1038/274581a0
- Martens, J., Wild, B., Pearce, C., Tesi, T., Andersson, A., Bröder, L., et al. (2018). Remobilization of old permafrost carbon to chukchi sea sediments during the end of the last deglaciation. *Global Biogeochem. Cycles* 33, 2–14. doi: 10.1029/2018GB005969
- März, C., Poulton, S. W., Brumsack, H.-J., and Wagner, T. (2012). Climate-controlled variability of iron deposition in the Central Arctic Ocean (southern Mendeleev Ridge) over the last 130,000years. *Chem. Geol.* 33, 116–126. doi: 10.1016/j.chemgeo.2012.08.015
- März, C., Stratmann, A., Matthiessen, J., Meinhardt, A.-K., Eckert, S., Schnetger, B., et al. (2011). Manganese-rich brown layers in arctic ocean sediments: composition, formation mechanisms, and diagenetic overprint. *Geochim. Cosmochim. Acta* 75, 7668–7687. doi: 10.1016/j.gca.2011.09.046
- McKinney, W. (2010). “Data structures for statistical computing in python,” in *Proceedings of the 9th Python in Science Conference*, eds S. van der Walt and J. Millman (Austin: SciPy Society), 51–56.
- Meinhardt, A.-K., März, C., Schuth, S., Lettmann, K. A., Schnetger, B., Wolff, J.-O., et al. (2016). Diagenetic regimes in arctic ocean sediments: implications for sediment geochemistry and core correlation. *Geochim. Cosmochim. Acta* 188, 125–146. doi: 10.1016/j.gca.2016.05.032
- Myers, C. R., and Nealon, K. H. (1988). Microbial reduction of manganese oxides: interactions with iron and sulfur. *Geochim. Cosmochim. Acta* 52, 2727–2732. doi: 10.1016/0016-7037(88)90041-5
- Nowaczyk, N. R., Frederichs, T. W., Eisenhauer, A., and Gard, G. (1994). Magnetostratigraphic data from late quaternary sediments from the yermak plateau, arctic ocean: evidence for four geomagnetic polarity events within the last 170 Ka of the brunhes chron. *Geophys. J. Int.* 117, 453–471. doi: 10.1111/j.1365-246x.1994.tb03944.x
- Nowaczyk, N. R., Frederichs, T. W., Kassens, H., Nørgaard-Pedersen, N., Spielhagen, R. F., Stein, R., et al. (2001). Sedimentation rates in the makarov basin, central arctic ocean: a paleomagnetic and rock magnetic approach. *Paleoceanography* 16, 368–389. doi: 10.1029/2000pa000521
- Nowaczyk, N. R., and Knies, J. (2000). Magnetostratigraphic results from the eastern Arctic Ocean: AMS 14 C ages and relative palaeointensity data of the Mono Lake and Laschamp geomagnetic reversal excursions. *Geophys. J. Int.* 140, 185–197. doi: 10.1046/j.1365-246x.2000.00001.x
- O’Regan, M., King, J., Backman, J., Jakobsson, M., Pälike, H., Moran, K., et al. (2008). Constraints on the pleistocene chronology of sediments from the lomonosov ridge. *Paleoceanography* 23:A1S19. doi: 10.1029/2007pa001551
- O’Reilly, W., and Banerjee, S. K. (1966). Oxidation of titanomagnetites and self-reversal. *Nature* 211:26. doi: 10.1038/211026a0
- Park, K., Kim, J.-H., Asahi, H., Polyak, L., Khim, B.-K., Schreck, M., et al. (2020). Cyclostratigraphic age constraining for quaternary sediments in the makarov basin of the western arctic ocean using manganese variability. *Quat. Geochronol.* 55:101021. doi: 10.1016/j.quageo.2019.101021
- Paterson, G. A., Zhao, X., Jackson, M., and Heslop, D. (2018). Measuring, processing, and analyzing hysteresis data. *Geochem. Geophys. Geosyst.* 19, 1925–1945. doi: 10.1029/2018GC007620
- Peters, C., and Dekkers, M. J. (2003). Selected room temperature magnetic parameters as a function of mineralogy, concentration and grain size. *Phys. Chem. Earth Parts A/B/C* 28, 659–667. doi: 10.1016/s1474-7065(03)00120-7
- Pokorný, J., Pokorný, P., Suza, P., and Hroudá, F. (2011). “A multi-function kappabridge for high precision measurement of the AMS and the variations of magnetic susceptibility with field, temperature and frequency,” in *The Earth\textquotesingles Magnetic Interior*, eds E. Petrovský, E. Herrero-Bervera, T. Harinarayana, and D. Ivers (Berlin: Springer), 293–301. doi: 10.1007/978-94-007-0323-0_20
- Polyak, L., Bischof, J., Ortiz, J. D., Darby, D. A., Channell, J. E. T., Xuan, C., et al. (2009). Late quaternary stratigraphy and sedimentation patterns in the western arctic ocean. *Global Planet. Change* 68, 5–17. doi: 10.1016/j.gloplacha.2009.03.014
- Polyak, L., Curry, W. B., Darby, D. A., Bischof, J., and Cronin, T. M. (2004). Contrasting glacial/interglacial regimes in the western Arctic Ocean as exemplified by a sedimentary record from the Mendeleev Ridge. *Palaeogeogr. Palaeoclimatol. Palaeoecol.* 203, 73–93. doi: 10.1016/s0031-0182(03)00661-8
- Roberts, A. P. (2015). Magnetic mineral diagenesis. *Earth-Sci. Rev.* 151, 1–47. doi: 10.1016/j.earscirev.2015.09.010
- Roberts, A. P., Tauxe, L., Heslop, D., Zhao, X., and Jiang, Z. (2018). A critical appraisal of the “day” diagram. *J. Geophys. Res. Solid Earth* 123, 2618–2644. doi: 10.1002/2017JB015247
- Roberts, A. P., and Winklhofer, M. (2004). Why are geomagnetic excursions not always recorded in sediments? Constraints from post-depositional remanent magnetization lock-in modelling. *Earth Planet. Sci. Lett.* 227, 345–359. doi: 10.1016/j.epsl.2004.07.040
- Rudels, B. (2009). *Arctic Ocean Circulation*. In *Encyclopedia of Ocean Sciences*. Amsterdam: Elsevier, 211–225. doi: 10.1016/b978-012374473-9.00601-9
- Schreck, M., Nam, S.-I., Polyak, L., Vogt, C., Kong, G.-S., Stein, R., et al. (2018). Improved pleistocene sediment stratigraphy and paleoenvironmental implications for the western Arctic Ocean off the East Siberian and Chukchi margins. *Arktos* 4:21. doi: 10.1007/s41063-018-0057-8
- Schulz, H. D., and Zabel, M. (eds). (2006). *Marine Geochemistry*, 2nd ed. Berlin: Springer-Verlag. doi: 10.1007/3-540-32144-6
- Schwämmle, V., and Jensen, O. N. (2010). A simple and fast method to determine the parameters for fuzzy c-means cluster analysis. *Bioinformatics* 26, 2841–2848. doi: 10.1093/bioinformatics/btq534
- Smirnov, A. V., and Tarduno, J. A. (2000). Low-temperature magnetic properties of pelagic sediments (Ocean Drilling Program Site 805C): tracers of maghemitization and magnetic mineral reduction. *J. Geophys. Res.* 105, 16457–16471. doi: 10.1029/2000jb900140
- Snowball, I., Almqvist, B., Lougheed, B. C., Wiers, S., Obrochta, S., and Herrero-Bervera, E. (2019). Coring induced sediment fabrics at IODP Expedition 347 Sites M0061 and M0062 identified by anisotropy of magnetic susceptibility (AMS): criteria for accepting palaeomagnetic data. *Geophys. J. Int.* 217, 1089–1107. doi: 10.1093/gji/ggz075
- Spielhagen, R. F., Baumann, K.-H., Erlenkeuser, H., Nowaczyk, N. R., Nørgaard-Pedersen, N., Vogt, C., et al. (2004). Arctic ocean deep-sea record of northern eurasian ice sheet history. *Quat. Sci. Rev.* 23, 1455–1483. doi: 10.1016/j.quascirev.2003.12.015
- Steuerwald, B. A., Clark, D. L., and Andrew, J. A. (1968). Magnetic stratigraphy and faunal patterns in Arctic ocean sediments. *Earth Planet. Sci. Lett.* 5, 79–85. doi: 10.1016/s0012-821x(68)80018-4

- van der Walt, S., Colbert, S. C., and Varoquaux, G. (2011). The NumPy array: a structure for efficient numerical computation. *Comput. Sci. Eng.* 13, 22–30. doi: 10.1109/MCSE.2011.37
- Warner, J., Sexauer, J., scikit-fuzzy, twmeggs, Alexander, M. S., Unnikrishnan, A., et al. (2017). JDWarner/scikit-fuzzy: scikit-Fuzzy 0.3.1 (Version 0.3.1). *Zenodo*. doi: 10.5281/zenodo.1002946
- Wiers, S., Snowball, I., O'Regan, M., and Almqvist, B. (2019). Late pleistocene chronology of sediments from the yermak plateau and uncertainty in dating based on geomagnetic excursions. *Geochem. Geophys. Geosyst.* 20, 3289–3310. doi: 10.1029/2018GC007920
- Xuan, C., and Channell, J. E. T. (2010). Origin of apparent magnetic excursions in deep-sea sediments from Mendeleev-Alpha Ridge, Arctic Ocean. *Geochem. Geophys. Geosyst.* 11, 1–17. doi: 10.1029/2009gc002879
- Ye, L., März, C., Polyak, L., Yu, X., and Zhang, W. (2019). Dynamics of manganese and cerium enrichments in arctic ocean sediments: a case study from the alpha ridge. *Front. Earth Sci.* 6:236. doi: 10.3389/feart.2018.00236
- Zijderveld, J. D. A. (1967). “AC demagnetization of rocks: analysis of results,” in *Methods in Palaeomagnetism*, eds S. K. Runcorn, K. M. Creer, and D. W. Collinson (Amsterdam: Elsevier), 254–286. doi: 10.1016/b978-1-4832-2894-5.50049-5

Conflict of Interest: The authors declare that the research was conducted in the absence of any commercial or financial relationships that could be construed as a potential conflict of interest.

Copyright © 2020 Wiers, Snowball, O'Regan, Pearce and Almqvist. This is an open-access article distributed under the terms of the Creative Commons Attribution License (CC BY). The use, distribution or reproduction in other forums is permitted, provided the original author(s) and the copyright owner(s) are credited and that the original publication in this journal is cited, in accordance with accepted academic practice. No use, distribution or reproduction is permitted which does not comply with these terms.